RESEARCH ARTICLE

Check for updates

Isomeric diazapyrene–thiophene conjugated systems: synthesis, characterization, and transport properties†

Honglei Li,[a,b] Guodong Zhao,[c] Qingxin Tang, [ID][c] Hongkun Tian [ID] *[a,b] and Lixiang Wang [ID][a,b]

Dihalogenated 4,9-diazapyrenes have been shown to be promising reactive intermediates that could be used to develop various diazapyrene-based π-conjugated systems and have great research prospects. Since pyrene chemistry is strongly position-dependent, two synthesis methods, *i.e.* post-functionalization (electrophilic substitution) and pre-functionalization (pre-introduction of halogen atoms), were developed to synthesize three dihalogenated diazapyrene molecules substituted at different sites. Then, three isomeric co-oligomers of diazapyrene and bithiophene (1,6-, 2,7- and 3,8-PyNN-T2) were obtained through Suzuki cross-coupling reactions. Their crystal structures, and optoelectronic and charge transport properties were investigated, which demonstrated distinct position-dependence. Among the three isomers, 3,8-PyNN-T2 exhibited hole mobility up to 1.14 cm^2 V^{-1} s^{-1}, as observed in single crystal organic field-effect transistors. Our work fills the gap in the study of halogenated diazapyrenes and provides powerful tools for further derivatization of diazapyrenes.

Introduction

Over the past decade, polycyclic (hetero) aromatic hydrocarbons (PAHs) have attracted much attention in materials science due to their excellent charge-transfer capabilities and tunable photophysical and electrochemical properties.[1–4] Pyrene, the simplest representative of a peri-condensed PAH, with intensive blue emission, pronounced π-stacking capability and very unique reactivity, is a widely investigated fluorogenic motif and a common building block used to construct expanded π-conjugated systems with high optoelectronic performance.[5–16] Thus, continuous efforts have been directed toward the promotion and expansion of usable methods for the synthesis of functionalized pyrene-based compounds.

Among them, doping of nitrogen atoms into pyrene frameworks could be considered as an effective strategy to regulate their intrinsic physicochemical properties, resulting in their application in the field of organic electronics, such as in organic solar cells (OSCs), organic light-emitting diodes (OLEDs), and organic field-effect transistors (OFETs).[17–21]

4,9-Diazapyrene, a typical nitrogen-containing pyrene with two nitrogen atoms at the K-region of the pyrene skeleton, possesses a packing motif with strong π–π interactions,[22] which makes it a noteworthy candidate for potential application in DNA intercalators, multi-stimuli-responsive smart materials, and optoelectronic devices.[23–25] However, literature on 4,9-diazapyrene and its conjugation-extended derivatives is limited, mainly due to challenges in synthesis. Moreover, the construction of π-conjugated materials with 4,9-diazapyrene as the building block usually requires different halogenated intermediates with selective substitution positions. It is of crucial importance to understand how to modulate their electronic, photophysical and charge-transfer properties. Thus, developing effective synthetic methods to obtain dihalogenated 4,9-diazapyrene with varying substitution sites is highly desirable and yet challenging.

Chen *et al.* reported the synthesis of a key intermediate, 2,7-dibromo-5,10-dimethyl-4,9-diazapyrene, through Bischler–Napieralski cyclization of the corresponding amide precursors.[24,26] Inspired by their method to construct the 4,9-diazapyrene core, we developed two effective synthesis strat-

[a]State Key Laboratory of Polymer Physics and Chemistry, Changchun Institute of Applied Chemistry, Chinese Academy of Sciences, Changchun, Jilin, 130022, P. R. China. E-mail: hktian@ciac.ac.cn
[b]School of Applied Chemistry and Engineering, University of Science and Technology of China, Hefei, Anhui, 230026, P. R. China
[c]Center for Advanced Optoelectronic Functional Materials Research and Key Lab of UV-Emitting Materials and Technology of Ministry of Education, Northeast Normal University, Changchun, Jilin, 130024 P. R. China

†Electronic supplementary information (ESI) available: Instruments, experimental details, characterization of OFET devices, TGA and DSC curves of these polymers and other device data. CCDC 2371376, 2371380 and 2371524. For ESI and crystallographic data in CIF or other electronic format see DOI: https://doi.org/10.1039/d4qo01305k
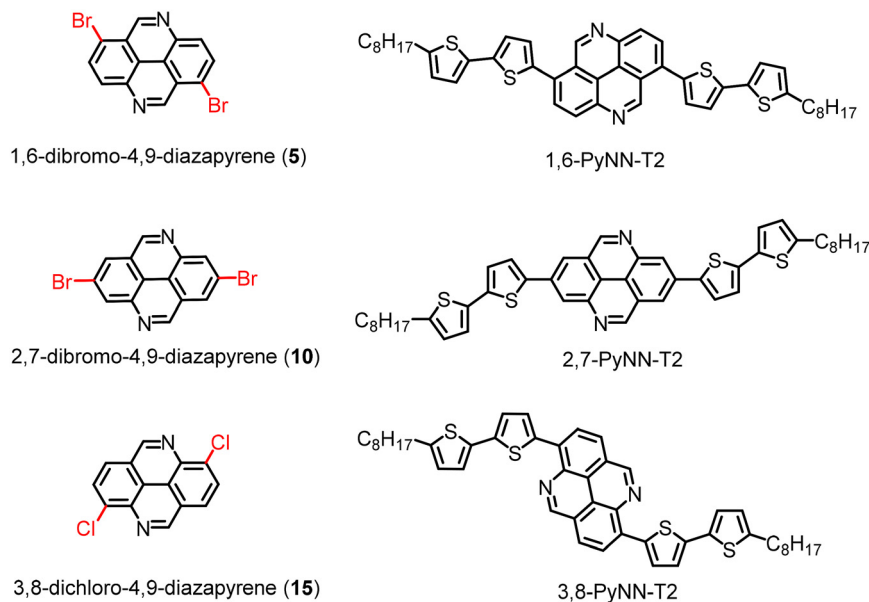
This journal is © the Partner Organisations 2024

Org. Chem. Front., 2024, **11**, 7205–7213 | **7205**

Chart 1 Chemical structures of the target 4,9-diazapyrene derivatives in this work.

egies, post-functionalization (electrophilic substitution of diazapyrene) and pre-functionalization (pre-introduction of halogen atoms), to obtain three different dihalogen-substituted diazapyrene compounds (1,6-dibromo, 2,7-dibromo and 3,8-dichloro-4,9-diazapyrenes), and then through Pd-catalyzed cross-coupling reactions, three isomerized co-oligomers of diazapyrene and bithiophene were also further designed and synthesized (Chart 1). Our work not only expands the chemical diversity of diazapyrene compounds but is also the first to report on the charge-transfer properties of diazapyrene-based π-conjugated systems. Since pyrene chemistry is strongly position-dependent, the present work contributes to a deeper understanding of the basic structure–property relationship of diazapyrene-based isomers.
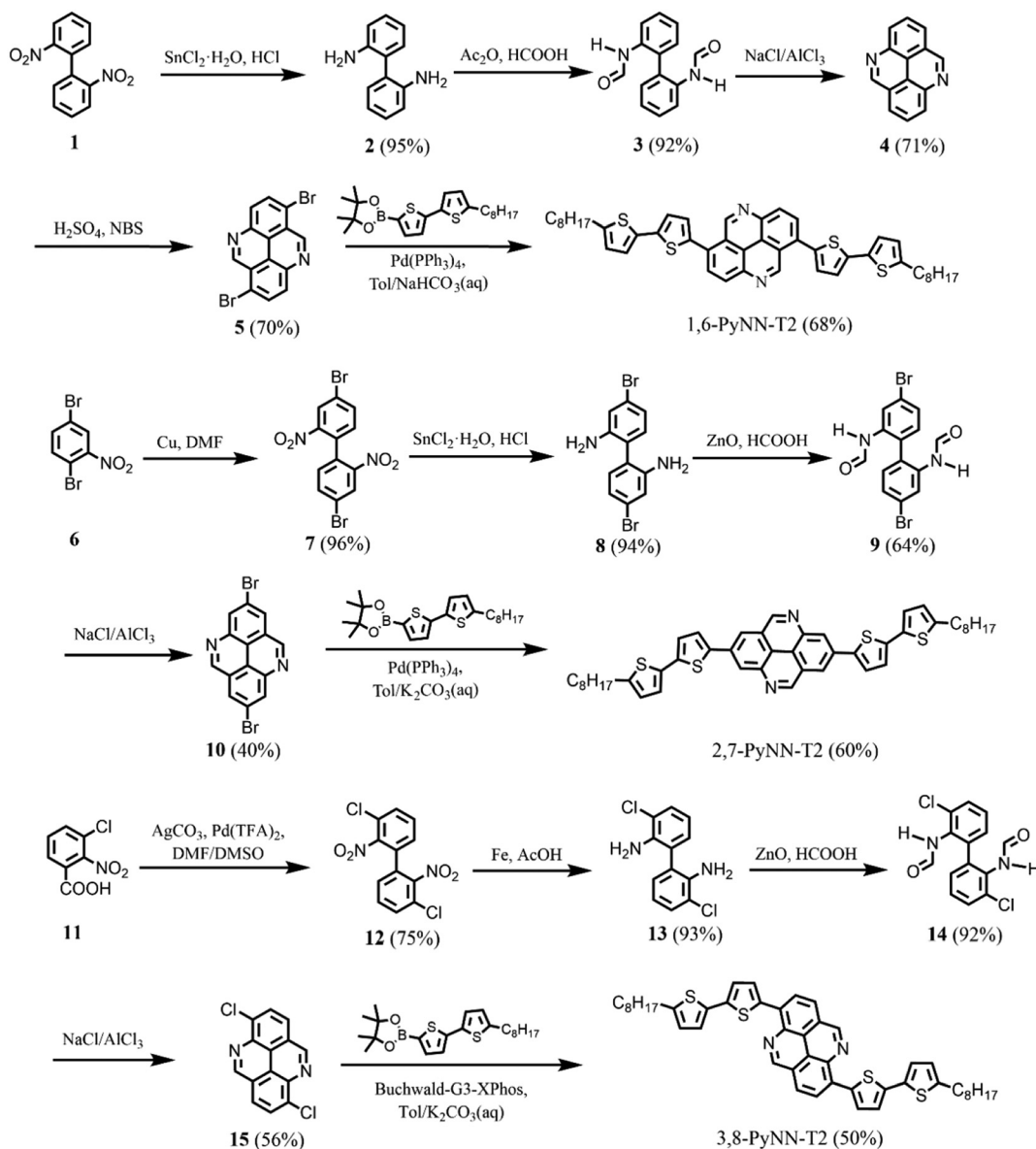
Results and discussion

Synthesis and structural characterization

Scheme 1 shows the synthesis routes for the target compounds, including three 4,9-diazapyrene molecules with different halogenated sites and the corresponding isomerized π-conjugated co-oligomers (1,6-, 2,7- and 3,8-PyNN-T2). Synthesis details and corresponding characterization spectra are described and shown in the ESI.† Since direct bromination of 4,9-diazapyrene has not been explored so far, we firstly synthesized 4,9-diazapyrene starting from commercially available 1-nitro-2-(2-nitrophenyl)benzene (**1**).[27] Through reduction with stannous chloride dehydrate and then acylation using acetic anhydride as an activator and formic acid as an acylation reagent, compounds **2** and **3** were obtained in high yields beyond 90%. Next, an ionic liquid (molten AlCl₃/NaCl) was used in the Bischler–Napieralski

cyclization to obtain 4,9-diazapyrene (**4**) in a yield of 71%. Finally, the bromination reaction was conducted using NBS in concentrated sulfuric acid, which resulted in the highly selective synthesis of 1,6-dibromo-4,9-diazapyrene (**5**) in a yield of 70% after recrystallization from chloroform. For 2,7-dibromo-4,9-diazapyrene, the synthesis route provided by Chen *et al.* was modified.[24] When acetic anhydride/formic acid was used to synthesize compound **9**, only a single-conversion product could be obtained. So, we further attempted to use zinc oxide as a catalyst and formic acid as an acylation reagent.[28] To our delight, we found that the double-conversion product **9** was achieved in a yield of 64%. Under the same Bischler–Napieralski cyclization conditions, 2,7-dibromo-4,9-diazapyrene (**10**) was obtained in a yield of 40%. Compound **12** was obtained using the dicarboxylic acid coupling method from the inexpensive commercial 3-chloro-2-nitrobenzoic acid **11**.[29] However, under the reduction conditions using stannous chloride dehydrate, the yield of compound **13** was relatively low because of the formation of a by-product, 4,7-dichlorobenzo[*c*]cinnoline. Therefore, iron powder was chosen as the reduction reagent, and no such by-product was found.[24] The yield of **13** could be improved to 93%. Then, acylation using zinc oxide/formic acid delivered compound **14** in a yield of 92%. Under the same Bischler–Napieralski cyclization conditions, 3,8-dichloro-4,9-diazapyrene (**15**) was obtained in a yield of 56%. After the successful synthesis of the three different dihalogen-substituted diazapyrene compounds, we proceeded to the synthesis of three isomerized π-conjugated co-oligomers as the final targets. Using Pd(PPh₃)₄ as the catalyst, Suzuki–Miyaura cross-coupling reactions of dibromo-diazapyrenes and 5-octyl-5′-[4,4,5,5-tetramethyl-1,3,2-dioxaborolanyl]-2,2′-bithiophene were carried out to obtain 1,6-PyNN-T2 and 2,7-PyNN-T2,

7206 | *Org. Chem. Front.*, 2024, **11**, 7205–7213

This journal is © the Partner Organisations 2024

Scheme 1 Synthetic routes to 1,6-PyNN-T2, 2,7-PyNN-T2, and 3,8-PyNN-T2.

respectively. Using Buchwald-G3-XPhos as the pre-catalyst, 3,8-PyNN-T2 molecule could be prepared from its corresponding dichloro-derivative.[30] The three isomerized co-oligomers were purified through double vacuum sublimation.

The structures of the three target molecules were verified by NMR spectroscopy, matrix-assisted laser desorption ionization time-of-flight mass spectrometry (MALDI-TOF MS), elemental analysis and single-crystal X-ray analysis (*vide infra*). Thermogravimetric analysis (TGA) and differential scanning calorimetry (DSC) were also performed. All compounds exhibited good thermal stability with a weight loss of 1% at approximately 420 °C (Fig. S30†), consistent with the behavior of the pyrene-based analogues such as 1,6-bis(5′-octyl-2,2′-bithiophen-5-yl)pyrene (BOBTP), which showed 1% loss of the mass at 408 °C.[31] As shown in the DSC curves, 1,6-PyNN-T2, 2,7-

PyNN-T2 and 3,8-PyNN-T2 exhibited melting points of 168, 150 and 204 °C, respectively (Fig. S31†).

Single crystal structure analysis

After many attempts, the single crystal structure of 1,6-PyNN-T2 was obtained by slow diffusion of methanol into its dilute chloroform solution at room temperature. The single crystals of 2,7-PyNN-T2 and 3,8-PyNN-T2 were obtained by slowly evaporating chlorobenzene solution under ambient conditions. They were used for X-ray crystal structure analysis. All of the crystallographic data are provided in Tables S1–3 (ESI†). The three isomeric co-oligomers exhibited distinct molecular configuration and packing motifs. For clarity, the octyl chains and H atoms were omitted. The structure of 1,6-PyNN-T2 was solved and refined in the triclinic *P*1̄ space group. As shown in

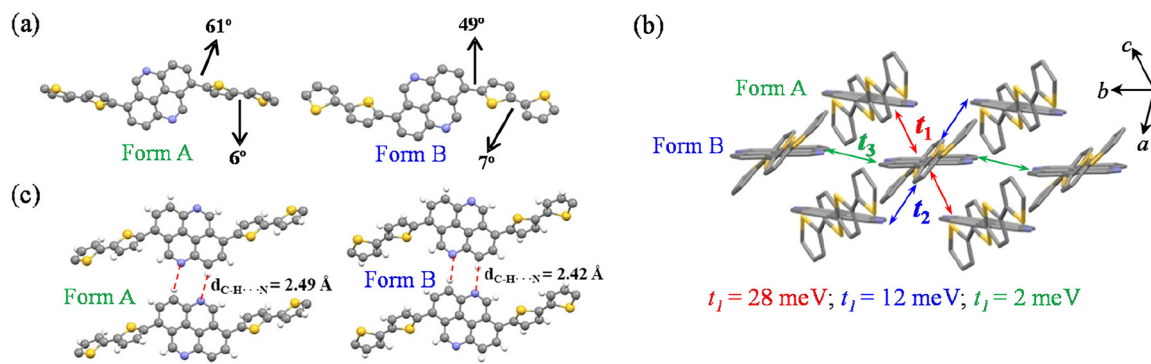This journal is © the Partner Organisations 2024

Org. Chem. Front., 2024, **11**, 7205–7213 | **7207**

Fig. 1 Molecular conjugated backbone configurations (a), the packing diagrams and transfer integrals (b) and the intermolecular C−H···N interactions (c) of 1,6-PyNN-T2.

Fig. 1a, the conjugated backbone of 1,6-PyNN-T2 showed large dihedral angles between the diazapyrene unit and thiophene unit of 61° and 49° for Form A and B, respectively, implying the poor conjugation of this molecule. Meanwhile, the dihedral angles between thiophene units were about of 6° for both forms. The molecules of 1,6-PyNN-T2 were packed in an unusual motif, as shown in Fig. 1b, in which the arrangement of the diazapyrene units was nearly parallel along the b axis and the bithiophene moieties form a herringbone packing motif in the ab plane. After further analysis, it is found that this packing motif was mainly driven by the formation of the C−H···N bonding network, resulting from the shorter contact distances of 2.49 Å (Form A) and 2.42 Å (Form B) than the sum of the van der Waals radii of the N and H atoms (2.70 Å), and large bond angles beyond 160°, as shown in Fig. 1c.

The molecule 2,7-PyNN-T2 crystallizes in a monoclinic ($P2_1/n$) structure. Different from the 1,6-PyNN-T2 molecule, 2,7-PyNN-T2 has an almost planar conjugated backbone, with a small dihedral angle of 7° between the diazapyrene unit and thiophene unit and 2° between thiophene units, as shown in

Fig. 2a. The former dihedral angle was similar to that of 2,7-bis(5-hextyl-thiophen-2-yl)pyrene (DHT-P).[32] These molecules packed in a slipped cofacial π–π stacking manner with an interplanar separation of 3.52 Å along the a axis.

3,8-PyNN-T2 crystals belong to the C/c space group. Noncovalent intramolecular N → S interactions were formed with the conjugated backbone, demonstrated by the shorter contact distances of ~2.8 Å (both Form A and B) than the sum of the van der Waals radii of N and S atoms (3.35 Å). This effect originates from the presence of the low-lying C–S σ* orbitals on S atoms, creating the phenomenon called σ-holes, which have a positive electrostatic potential and are available for interaction with electron-donating atoms, especially N and O.[33] Compared to the 1,6-isomer, the trade-off of the locking effect of N → S interactions and the repulsive effect of spatially adjacent H-atoms made the smaller dihedral angles of ~12° between the diazapyrene unit and thiophene unit. The 3,8-PyNN-T2 moieties pack in a herringbone (HB) motif in the ab plane with a T-shaped HB angle of approximately 34° (determined from the dihedral angle between the least-squares
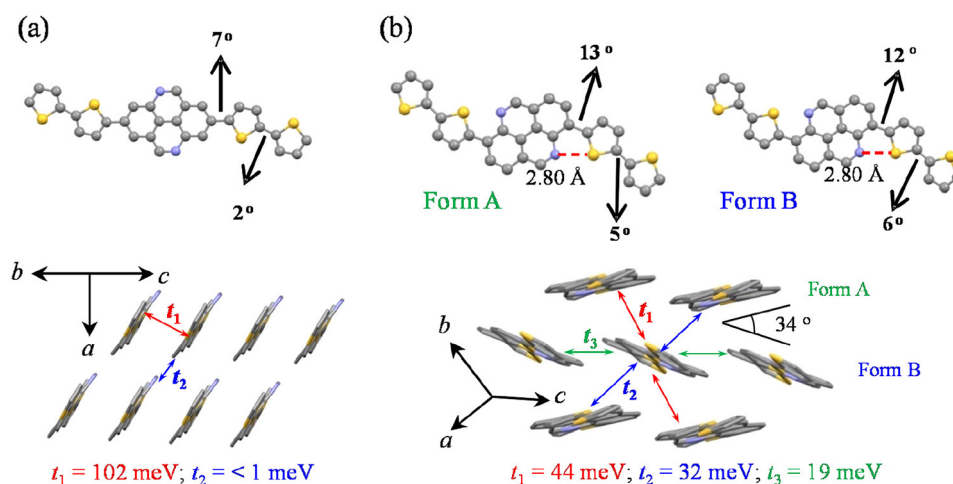

Fig. 2 Molecular conjugated backbone configuration (top) and the packing structure diagrams and transfer integrals (bottom) of 2,7-PyNN-T2 (a) and 3,8-PyNN-T2 (b).

7208 | *Org. Chem. Front.*, 2024, **11**, 7205–7213

This journal is © the Partner Organisations 2024

planes of the nearest neighbours including all non-hydrogen atoms in one molecule), as shown in Fig. 2b.

Based on the packing structures of the three isomeric molecules, the transfer integral (t) values were calculated to investigate the potential charge-transport capability as p-type organic semiconductors (*vide infra*).[34–36] It was found that the molecular configurations and packing structures have significant impact on transfer integrals. As expected from the 1D π–π stacking structure of 2,7-PyNN-T2 with its almost planar backbone, the larger t of 102 meV (t_1) can be formed in the π–π stacking direction, indicating 1D charge-transport capability. The 1,6-PyNN-T2 had a significantly larger t value of 28 meV (t_1) and 12 meV (t_2) in the transverse direction but only 2 meV (t_3) along the column direction. This situation may have originated from the obvious distorted conjugated backbone and would result in anisotropic 2D charge-transport properties. Meanwhile, the HB molecular arrangement of 3,8-PyNN-T2 with a more planar backbone configuration results in a larger t in the transverse and column directions (t_1 = 44 meV, t_2 = 32 meV and t_3 = 19 meV) than those of the 1,6-isomer, demonstrating favorable 2D charge-transport properties.

Photophysical and electrochemical properties

The photophysical properties of these PyNN-T2 molecules were studied using UV-visible absorption spectroscopy (Fig. 3a). The spectra of their diluted chloroform solutions showed two absorption bands. The higher energy transitions (presumably π → π⋆) can be observed in the range of 300–350 nm, while the lower energy transitions (presumably n → π⋆) can be found in the spectral range between 350 and 500 nm. The n → π⋆ transition can be associated with the presence of heteroatoms (S or N) within the conjugated backbones.[37,38] Depending on the different substituted positions of 4,9-diazapyrene, distinct absorption behaviours can be observed for the three isomers. 1,6-, 2,7- and 3,8-PyNN-T2 have two peaks at 321 and 448 nm, 339 and 393 nm, and 328 and 492 nm, respectively (Table 1). The corresponding optical band gaps (E_g) were estimated from the onset of the UV–vis absorption spectra as 2.43, 2.72, and 2.21 eV, respectively. The pyrene-based analogue BOBTP also showed two absorption peaks at 322 nm and 410 nm in a diluted chloroform solution, with E_g of 2.52 eV.[31] These results suggested that the incorporation of nitrogen atoms could reduce the energy gap in analogous diazapyrene derivatives. Compared to their behaviour in the solution phase, the absorption peaks exhibited a certain degree of blue shift in the thin film. Among the three co-oligomers, the shift of 3,8-PyNN-T2 is the largest and is approximately 60 nm, while the shifts are about 20 and 10 nm for 1,6- and 2,7-PyNN-T2, respectively. This phenomenon could be attributed to the formation of H-aggregation in the films, which was usually
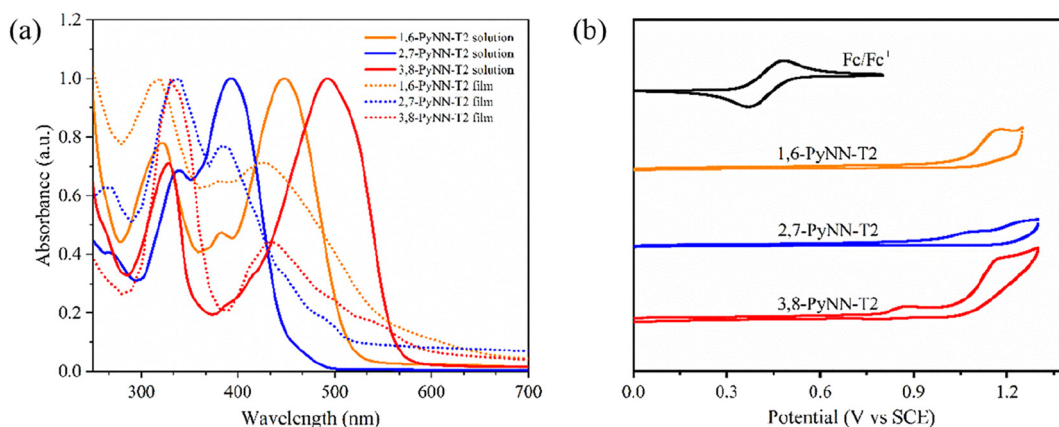

Fig. 3 UV-vis absorption spectroscopy of 1,6, 2,7- and 3,8-PyNN-T2 in CHCl₃ (1 × 10⁻⁵ M) (a) and cyclic voltammograms of 1,6-, 2,7- and 3,8-PyNN-T2 measured in CH₂Cl₂ with 0.1 M Bu₄NPF₆ as electrolyte (b).

Table 1 Thermal, photophysical and electrochemical properties of 1,6-PyNN-T2, 2,7-PyNN-T2 and 3,8-PyNN-T2

Compound	T_m [a] [°C]	T_d [b] [°C]	λ_{max} [nm] Solution	λ_{max} [nm] Film	E_g [c] [eV]	E_{HOMO} [d] [eV]	E_{LUMO} [e] [eV]
1,6-PyNN-T2	168	424	321, 448	320, 430	2.43	−5.40	−2.97
2,7-PyNN-T2	150	425	339, 393	340, 380	2.72	−5.34	−2.62
3,8-PyNN-T2	204	424	328, 492	330, 430	2.21	−5.17	−2.96

[a] Melting point determined from DSC heating curves. [b] 1% weight loss temperature determined from TGA measurements. [c] Optical energy gaps (E_g) calculated from solution spectra according to the equation $E_g = 1240/\lambda_{onset}$ eV. [d] Calculated according to $E_{HOMO} = -(4.80 + E_{ox}^{onset})$ eV, where E_{ox}^{onset} represents oxidation onset, *versus* Fc/Fc⁺ couple. [e] $E_{LUMO} = E_g - E_{HOMO}$.

This journal is © the Partner Organisations 2024

Org. Chem. Front., 2024, **11**, 7205–7213 | **7209**

related to exciton coupling between adjacent molecules in close-packed structures, as revealed by crystal structure analysis. Moreover, the varying degrees of blue shift presumably implied the different extent of intermolecular interactions.

The electrochemical properties of three isomers were studied by cyclic voltammetry (CV). Fig. 3b shows their irreversible oxidation peaks in CH_2Cl_2 solutions, which indicates that electron transfer at the electrode surface is slower compared to mass transport and even if there are electrochemically reactive substances present on the surface of the work electrode, it is difficult to them to react completely.[39] Some diazapyrene derivatives and pyrene–thiophene derivatives also exhibited this irreversible oxidation characteristic.[24,31,32] Accordingly, the HOMO energy levels of 1,6-, 2,7- and 3,8-PyNN-T2 were calculated as −5.40, −5.34, and −5.17 eV (Table 1), respectively, from the onset oxidation potential with reference to Fc^+/Fc (−4.8 eV). The LUMO energy levels were calculated based on the absorption edges, and were −2.97, −2.62 and −2.96 eV, respectively. The low-lying HOMO and LUMO energy levels of diazapyrene-based co-oligomers demonstrate their potential application as p-type semiconductors.[40,41]

Density functional theory calculations

In order to further understand their electronic structure, the electronic distribution of the HOMO and LUMO of the three molecules was calculated at the B3LYP/6-31G(d,p) level using Gaussian 09 software. For simplifying the calculations, long octyl chains were replaced with methyl groups. The optimized molecular geometries and HOMO and LUMO distribution diagrams of the three molecules are shown in Fig. 4. The 1,6-substituted molecule exhibited partial distortion with torsion angles of 44° between the diazapyrene unit and thiophene unit, and 17° between the thiophene units in the gas state. In contrast, the 2,7- and 3,8-PyNN-T2 molecules exhibited planar structures. For 1,6- and 3,8-PyNN-T2 molecules, the HOMO and LUMO delocalized over the whole molecule. For the 2,7-PyNN-T2 molecule, the electron density distribution of the HOMO is also delocalized similar to that of the first two, while that of the LUMO localized in the central diazapyrene portion. Depending on the different substituted positions of 4,9-diazapyrene, the HOMO levels increased in the order of 1,6-, 2,7- and 3,8-PyNN-T2. Meanwhile, the LUMO levels decreased in the order of 2,7-, 1,6- and 3,8-PyNN-T2. Following this change in trend, the 3,8-PyNN-T2 molecule exhibited the narrowest band gap, which was also in good agreement with the experimental results.

Charge transport properties

To characterize the semiconducting charge carrier transfer properties of the three isomeric molecules, bottom-gate and top-contact organic field-effect transistor (OFET) devices were fabricated on the octadecyltrimethoxysilane (OTMS)-modified SiO_2/Si substrates by vapor deposition at the optimal substrate temperature (T_S). Details of device fabrication can be found in the ESI.† The OTFTs were measured under ambient conditions in the dark. Neither 1,6-PyNN-T2 nor 2,7-PyNN-T2 displayed measurable field effect characteristics, despite the fact that their calculated HOMO energy levels and transfer integrals from single crystal data appear favorable for p-channel transport. The out-of-plane and in-plane XRD patterns for 1,6- and 2,7-PyNN-T2 films are shown in Fig. S34.† Compared to the single crystal diffraction data, the packing structures of both molecules in the films were different from those in the single crystals, which may have a negative impact on charge carrier transfer. In addition, the nonplanar π-conjugated molecular geometry of 1,6-PyNN-T2 molecules may inhibit effective intermolecular interactions in the process of film formation. Moreover, AFM studies of films of 2,7-PyNN-T2 revealed a morphology that does not seem to be suited for conduction (see the ESI†). All OFETs based on vacuum deposited 3,8-PyNN-T2 molecules exhibited p-type transport characteristics (Fig. 5a and S32a†). As listed in Table S4,† the highest hole
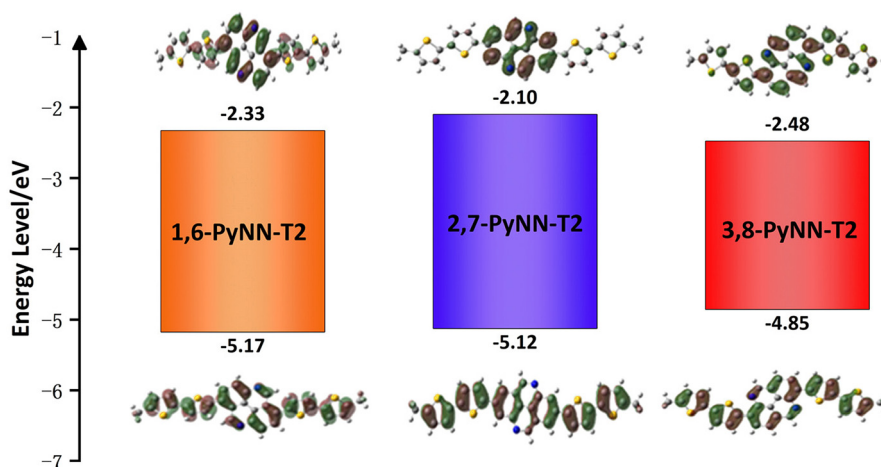

Fig. 4 Calculated molecular orbitals and frontier orbital levels of 1,6-PyNN-T2, 2,7-PyNN-T2 and 3,8-PyNN-T2. The calculation was performed at the B3LYP/6-31G(d,p) level.
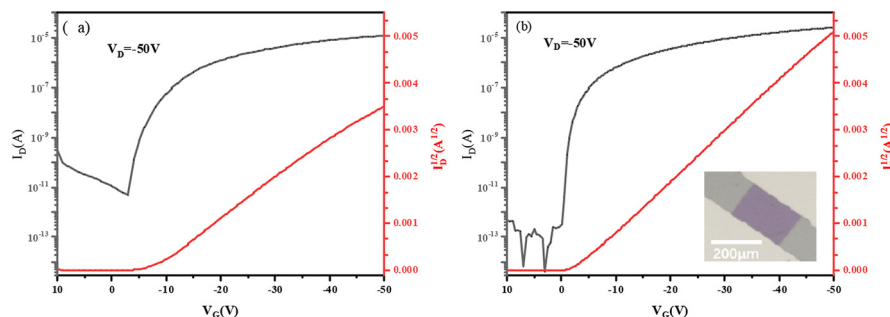
7210 | *Org. Chem. Front.*, 2024, **11**, 7205–7213

This journal is © the Partner Organisations 2024

Fig. 5 Typical transfer characteristics of OFET with vacuum deposited 3,8-PyNN-T2 (a) and single-crystal OFET device based on 3,8-PyNN-T2 with its optical microscopy image (b).

mobility of the OFET devices with 3,8-PyNN-T2 was up to 0.17 cm^2 V^{-1} s^{-1} at T_S of 90 °C, along with a threshold voltage (V_T) of −7 V. The high hole mobility of 3,8-PyNN-T2 is consistent with its better molecular planarity and favorable 2D packing structure compared to the other two isomers. The diffraction peaks of the films of 3,8-PyNN-T2 largely resembled those of the bulk single crystal. As shown in Fig. 6a, two peaks at 2θ = 2.7 and 5.3° appeared in the out-of-plane direction with a d-spacing of 33.3 and 16.7 Å, which was close to half of the c-axis length obtained from the single crystal data. They could be assigned as (002) and (004), indicating that the ab plane was parallel to the substrate surface. Furthermore, from the in-plane diffraction patterns (Fig. 6b), two peaks at 2θ = 16.5 and 23.1° can be assigned to (023) and (220), which are from HB packing along the column and transverse directions. The peak at 2θ = 20.6° with a d-spacing of 4.3 Å originated from the ordered alkyl chain stacking. The micro/nano-sized single crystal devices, as shown in Fig. S33 and Table S5,† were further fabricated to improve charge transport capability due to the low trap density. The typical transfer and output curves of single crystal OFET devices are shown in Fig. 5b and S32b† and they exhibited almost ideal transfer characteristics. The

highest mobility was up to 1.14 cm^2 V^{-1} s^{-1}. Meanwhile, it could also be observed that single crystal devices have a lower V_T of −2 V than the devices fabricated by vapor deposition. To the best our knowledge, the charge transfer properties of 3,8-PyNN-T2 are the first reported so far for a diazapyrene-based conjugated system.

Conclusion

In summary, we have developed a new strategy to synthesize three different dihalogenated (Br or Cl) 4,9-diazapyrenes, which involves post-functionalization (direct electrophilic substitution of diazapyrene) and pre-functionalization (pre-introduction of halogen atoms) by the Bischler–Napieralski cyclization of rationally designed amide precursors. Based on these valuable intermediates, three isomeric co-oligomers of 4,9-diazapyrene and dithiophene were prepared by Suzuki–Miyaura cross-coupling reactions. Single crystals suited for X-ray diffraction have been grown, revealing polymorphism for the three compounds. Depending on the different substituted positions of 4,9-diazapyrene, the three isomers exhibited distinct absorption behaviours and electronic energy structures, as determined by UV-vis absorption spectroscopy, cyclic voltammetry and DFT calculations. Single-crystal OFETs have been fabricated and the highest hole mobility of 1.14 cm^2 V^{-1} s^{-1} was obtained for 3,8-PyNN-T2. As we have shown in this first study, the 4,9-diazapyrene molecules have potential for further derivatization, paving the way for accessing novel organic semiconductors.

Data availability

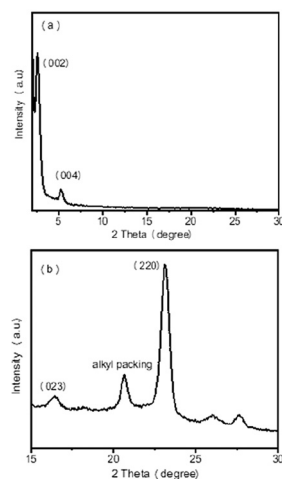The authors confirm that the data supporting the findings of this study are available in the ESI.†

Fig. 6 Out-of-plane (a) and in-plane (b) X-ray diffraction (XRD) patterns of 3,8-PyNN-T2 thin film prepared by vacuum deposition.

Conflicts of interest

There are no conflicts to declare.

This journal is © the Partner Organisations 2024

Org. Chem. Front., 2024, **11**, 7205–7213 | **7211**

Acknowledgements

References

1 A. Borissov, Y. K. Maurya, L. Moshniaha, W.-S. Wong, M. Żyła-Karwowska and M. Stępień, Recent Advances in Heterocyclic Nanographenes and Other Polycyclic Heteroaromatic Compounds, *Chem. Rev.*, 2021, **122**, 565–788.

2 X.-Y. Wang, X. Yao, A. Narita and K. Müllen, Heteroatom-Doped Nanographenes with Structural Precision, *Acc. Chem. Res.*, 2019, **52**, 2491–2505.

3 M. Stępień, E. Gońka, M. Żyła and N. Sprutta, Heterocyclic Nanographenes and Other Polycyclic Heteroaromatic Compounds: Synthetic Routes, Properties, and Applications, *Chem. Rev.*, 2017, **117**, 3479–3716.

4 C. Wang, H. Dong, W. Hu, Y. Liu and D. Zhu, Semiconducting π-Conjugated Systems in Field-Effect Transistors: A Material Odyssey of Organic Electronics, *Chem. Rev.*, 2011, **112**, 2208–2267.

5 X. Feng, X. Wang, C. Redshaw and B. Z. Tang, Aggregation Behaviour of Pyrene-based Luminescent Materials, from Molecular Design and Pptical Properties to Application, *Chem. Soc. Rev.*, 2023, **52**, 6715–6753.

6 T. M. Figueira-Duarte and K. Müllen, Pyrene-Based Materials for Organic Electronics, *Chem. Rev.*, 2011, **111**, 7260–7314.

7 X. Chang, Z. Zhou, C. Shang, G. Wang, Z. Wang, Y. Qi, Z.-Y. Li, H. Wang, L. Cao, X. Li, Y. Fang and P. J. Stang, Coordination-Driven Self-Assembled Metallacycles Incorporating Pyrene: Fluorescence Mutability, Tunability, and Aromatic Amine Sensing, *J. Am. Chem. Soc.*, 2019, **141**, 1757–1765.

8 S. Hu, L. Hu, X. Zhu, Y. Wang and M. Liu, Chiral V–shaped Pyrenes: Hexagonal Packing, Superhelix, and Amplified Chiroptical Performance, *Angew. Chem., Int. Ed.*, 2021, **60**, 19451–19457.

9 Y. Liu, L. Yang, Q. Bai, W. Li, Y. Zhang, Y. Fu and F. Ye, Highly Efficient Nondoped Blue Electroluminescence Based on Hybridized Local and Charge-transfer Emitter Bearing Pyrene-Imidazole and Pyrene, *Chem. Eng. J.*, 2021, **420**, 129939.

10 Y. Kou, G. Li, Y. Han, M. Li, T. Wang, Z. Qu and Y. Chen, Angularly Fused Diaza-dinaphthopyrenes: Regio-selective Synthesis, Crystal Structures and Isomer-dependent Mechanochromic Fluorescent Properties, *Chem. Sci.*, 2023, **14**, 668–674.

11 G. Cai, P. Xue, Z. Chen, T. Li, K. Liu, W. Ma, J. Lian, P. Zeng, Y. Wang, R. P. S. Han and X. Zhan, High-Performance Mid-Bandgap Fused-Pyrene Electron Acceptor, *Chem. Mater.*, 2019, **31**, 6484–6490.

12 Y. Wang, B. Liu, C. W. Koh, X. Zhou, H. Sun, J. Yu, K. Yang, H. Wang, Q. Liao, H. Y. Woo and X. Guo, Facile Synthesis of Polycyclic Aromatic Hydrocarbon (PAH)–Based Acceptors with Fine–Tuned Optoelectronic Properties: Toward Efficient Additive–Free Nonfullerene Organic Solar Cells, *Adv. Energy Mater.*, 2019, **9**, 1803976.

13 S. Liu, W. Su, X. Zou, X. Du, J. Cao, N. Wang, X. Shen, X. Geng, Z. Tang, A. Yartsev, M. Zhang, W. Gruber, T. Unruh, N. Li, D. Yu, C. J. Brabece and E. Wang, The Role of Connectivity in Significant Bandgap Narrowing for Fused-pyrene Based Non-fullerene Acceptors toward High-efficiency Organic Solar Cells, *J. Mater. Chem. A*, 2020, **8**, 5995–6003.

14 G.-L. Yang, Y. Xie, Z.-H. Jiao, J. Zhao, S.-L. Hou, Y. Shi, J. Han and B. Zhao, A Strong-alkali Resistant Zinc–organic Framework with 1,3,6,8-Tetra(pyridin-4-yl)pyrene for Efficient Photocatalytic Hydrogen Evolution, *J. Mater. Chem. A*, 2023, **11**, 16255–16262.

15 C. Zhou, W. Gu, G. Zhang, L. Liu, A. Lv and L. Zhang, Isomeric Pyrenodithiophenediones and Their Derivatives: Synthesis, Reactivity, and Device Performance, *J. Org. Chem.*, 2019, **84**, 5936–5942.

16 P. Gómez, J. Cerdá, M. Más-Montoya, S. Georgakopoulos, I. da Silva, A. García, E. Ortí, J. Aragó and D. Curiel, Effect of Molecular Geometry and Extended Conjugation on the Performance of Hydrogen-bonded Semiconductors in Organic Thin-film Field-Effect Transistors, *J. Mater. Chem. C*, 2021, **9**, 10819–10829.

17 A. Mukherjee, A. A. Akulov, S. Santra, M. V. Varaksin, G. A. Kim, D. S. Kopchuk, O. S. Taniya, G. V. Zyryanov and O. N. Chupakhin, 2,7-Diazapyrenes: a Brief Review on Synthetic Strategies and Application Opportunities, *RSC Adv.*, 2022, **12**, 9323–9341.

18 O. S. Taniya, A. F. Khasanov, M. V. Varaksin, E. S. Starnovskaya, A. P. Krinochkin, M. I. Savchuk, D. S. Kopchuk, I. S. Kovalev, G. A. Kim, E. V. Nosova, G. V. Zyryanov and O. N. Chupakhin, Azapyrene-based Fluorophores: Synthesis and Photophysical Properties, *New J. Chem.*, 2021, **45**, 20955–20971.

19 I. V. Borovlev and O. P. Demidov, Diazapyrenes, *Chem. Heterocycl. Compd.*, 2003, **39**, 1417–1442.

20 A. Vardanyan, M. A. Argüello Cordero, S. Lochbrunner, A. Villinger, P. Ehlers and P. Langer, Synthesis and Properties of 4- and 10-Benzoyl-1-azapyrenes, *J. Org. Chem.*, 2024, **89**, 2155–2168.

21 S. Geib, S. C. Martens, U. Zschieschang, F. Lombeck, H. Wadepohl, H. Klauk and L. H. Gade, 1,3,6,8-Tetraazapyrenes: Synthesis, Solid-State Structures, and Properties as Redox-Active Materials, *J. Org. Chem.*, 2012, **77**, 6107–6116.

22 R. Kiralj, B. Kojić-Prodić, I. Piantanida and M. Žinić, Crystal and Molecular Structures of Diazapyrenes and a Study of π⋯π Interactions, *Acta Chem. Scand., Ser. B*, 1999, **55**, 55–69.

7212 | *Org. Chem. Front.*, 2024, **11**, 7205–7213

This journal is © the Partner Organisations 2024

23 I. Piantanida, V. Tomišić and M. Žinić, 4,9-Diazapyrenium Cations. Synthesis, Physico-chemical Properties and Binding of Nucleotides in Water, *J. Chem. Soc., Perkin Trans. 2*, 2000, 375–383.

24 Y. Han, Z. Hu, M. Liu, M. Li, T. Wang and Y. Chen, Synthesis, Characterization, and Properties of Diazapyrenes via Bischler–Napieralski Reaction, *J. Org. Chem.*, 2019, **84**, 3953–3959.

25 C. Liang, M. Li and Y. Chen, Amphiphilic Diazapyrenes with Multiple Stimuli-Responsive Properties, *ACS Appl. Mater. Interfaces*, 2021, **13**, 20698–20707.

26 M. Li, Y. Yuan and Y. Chen, Bischler–Napieralski Cyclization: A Versatile Reaction towards Functional Aza–PAHs and Their Conjugated Polymers, *Chin. J. Chem.*, 2021, **39**, 3101–3115.

27 H. Klaasen, L. Liu, H.-Y. Gao, L. Viergutz, P. A. Held, T. Knecht, X. Meng, M. C. Börner, D. Barton, S. Amirjalayer, J. Neugebauer, A. Studer and H. Fuchs, Intermolecular Coupling and Intramolecular Cyclization of Aryl Nitriles on Au(111), *Chem. Commun.*, 2019, **55**, 11611–11614.

28 M. Hosseini-Sarvari and H. Sharghi, ZnO as a New Catalyst for N-Formylation of Amines under Solvent-Free Conditions, *J. Org. Chem.*, 2006, **71**, 6652–6654.

29 J. Cornella, H. Lahlali and I. Larrosa, Decarboxylative Homocoupling of (Hetero)aromatic Carboxylic Acids, *Chem. Commun.*, 2010, **46**, 8276–8278.

30 T. Kinzel, Y. Zhang and S. L. Buchwald, A New Palladium Precatalyst Allows for the Fast Suzuki-Miyaura Coupling Reactions of Unstable Polyfluorophenyl and 2-Heteroaryl Boronic Acids, *J. Am. Chem. Soc.*, 2010, **132**, 14073–14075.

31 H. Cho, S. Lee, N. S. Cho, G. E. Jabbour, J. Kwak, D.-H. Hwang and C. Lee, High-Mobility Pyrene-Based Semiconductor for Organic Thin-Film Transistors, *ACS Appl. Mater. Interfaces*, 2013, **5**, 3855–3860.

32 Y. Qiao, J. Zhang, W. Xu and D. Zhu, Novel 2,7-Substituted Pyrene Derivatives: Syntheses, Solid-state Structures, and Properties, *Tetrahedron*, 2011, **67**, 3395–3405.

33 B. R. Beno, K.-S. Yeung, M. D. Bartberger, L. D. Pennington and N. A. Meanwell, A Survey of the Role of Noncovalent Sulfur Interactions in Drug Design, *J. Med. Chem.*, 2015, **58**, 4383–4438.

34 E. F. Valeev, V. Coropceanu, D. A. da Silva Filho, S. Salman and J.-L. Brédas, Effect of Electronic Polarization on Charge-Transport Parameters in Molecular Organic Semiconductors, *J. Am. Chem. Soc.*, 2006, **128**, 9882–9886.

35 J. S. Huang and M. Kertesz, Intermolecular Transfer Integrals for Organic Molecular Materials: Can Basis Set Convergence Be Achieved?, *Chem. Phys. Lett.*, 2004, **390**, 110–115.

36 X. D. Yang, L. J. Wang, C. L. Wang, W. Long and Z. G. Shuai, Influences of Crystal Structures and Molecular Sizes on the Charge Mobility of Organic Semiconductors: Oligothiophenes, *Chem. Mater.*, 2008, **20**, 3205–3211.

37 K. R. Idzik, P. J. Cywiński, W. Kuznik, J. Frydel, T. Licha and T. Ratajczyk, The Pptical Properties and Quantum Chemical Calculations of Thienyl and Furyl Derivatives of Pyrene, *Phys. Chem. Chem. Phys.*, 2015, **17**, 22758–22769.

38 K. R. Idzik, T. Licha, V. Lukeš, P. Rapta, J. Frydel, M. Schaffer, E. Taeuscher, R. Beckert and L. Dunsch, Synthesis and Optical Properties of Various Thienyl Derivatives of Pyrene, *J. Fluoresc.*, 2013, **24**, 153–160.

39 N. Elgrishi, K. J. Rountree, B. D. McCarthy, E. S. Rountree, T. T. Eisenhart and J. L. Dempsey, A Practical Beginner's Guide to Cyclic Voltammetry, *J. Chem. Educ.*, 2018, **95**, 197–206.

40 X. Y. Wang, H. R. Lin, T. Lei, D. C. Yang, F. D. Zhuang, J. Y. Wang, S. C. Yuan and J. Pei, Azaborine Compounds for Organic Field–Effect Transistors: Efficient Synthesis, Remarkable Stability, and BN Dipole Interactions, *Angew. Chem., Int. Ed.*, 2013, **52**, 3117–3120.

41 J. Wen, F. Qiu, H. Liu, X. Liu, H. Hu, Y. Duan, Z. Wang and L. Zhang, syn/anti–Oligothienoacene Diimides with up to 10 Fused Rings, *Angew. Chem., Int. Ed.*, 2021, **61**, e202112482.

This journal is © the Partner Organisations 2024

Org. Chem. Front., 2024, **11**, 7205–7213 | **7213**